Scientific Research Publishing

Advances in Remote Sensing, 2026, 15(2), 40-62
https://www.scirp.org/journal/ars
ISSN Online: 2169-2688
ISSN Print: 2169-267X

Estimating Soil Moisture at Different Depths Using Multiple Satellite-Derived Indices

Eniola E. Olakanmi, Lydia E. Ebbuah, Souleymane Fall, Joseph E. Quansah*

Department of Agricultural and Environmental Sciences, Tuskegee University, Tuskegee, AL, USA
Email: eolakanmi6097@tuskegee.edu, lebbuah6888@tuskegee.edu, sfall@tuskegee.edu, *jquansah@tuskegee.edu

How to cite this paper: Olakanmi, E.E., Ebbuah, L.E., Fall, S. and Quansah, J.E. (2026) Estimating Soil Moisture at Different Depths Using Multiple Satellite-Derived Indices. *Advances in Remote Sensing*, **15**, 40-62.
https://doi.org/10.4236/ars.2026.152003

Received: March 16, 2026
Accepted: June 1, 2026
Published: June 4, 2026

Abstract

Understanding soil moisture dynamics at different depths is essential for irrigation management. This study evaluated the relationship between two satellite-derived moisture indices—the Normalized Difference Moisture Index (NDMI) and the Moisture Stress Index (MSI) and *in-situ* soil moisture measurements across the Alabama Black Belt region during the growing season. Soil moisture readings at depths of 15, 20, 25, and 30 cm were collected at five sensor locations between August 2023 and October 2025. Landsat 8/9 and Sentinel-2 imagery were processed to generate the moisture indices, which were then correlated with the sensor measurements. The results showed that, although both satellite data types had similar predictive performance for soil moisture at all depths, there were weak linear correlations at 15 - 20 cm that substantially increased at 25 - 30 cm. Landsat 8/9 soil moisture estimates were most accurate at 30 cm for both NDMI and MSI indices, whereas Sentinel-2 estimates were optimal at depths of between 25 and 30 cm. Both indices produced optimal correlations in the range of $r \approx 0.60$ - 0.64. These results demonstrate that satellite-based moisture indices exhibit statistically significant relationships with subsurface soil moisture conditions, particularly at depths greater than 25 cm, necessary for agricultural water management.

Keywords

Soil Moisture, Landsat, Sentinel, NDMI, MSI, Remote Sensing, Soil Sensor

1. Introduction

Soil moisture is a fundamental regulator of plant growth, nutrient uptake, canopy temperature, and overall crop productivity. It influences evapotranspiration processes and soil-plant-atmosphere interactions. Accurate soil moisture information is essential for agricultural water management and optimizing crop yield [1]-[3].

An understanding of soil moisture dynamics allows farmers to reduce irrigation waste, limit the risk of drought and excess water, and improve decision-making at the field and farm scale [4] [5]. However, the lack of reliable, detailed soil moisture data has limited farmers' capacity to make real-time, data-driven decisions on irrigation and water-use management [6]-[9].

Although conventional *in-situ* soil moisture sensors provide accurate point measurements, they are costly to deploy at a large scale, difficult to maintain, and impractical for large agricultural fields [10]-[13]. These constraints have encouraged the development of alternative approaches, including machine learning-based predictive models to improve soil moisture [14]-[17]. However, these models often require dense, high-quality training data, making them difficult to generalize across diverse soil types or management systems [11] [18].

Remote sensing has emerged as a powerful tool for estimating soil biophysical properties, including soil moisture. It provides vast information on the spatial and temporal properties of soils [11] [15] [19] [20]. The National Aeronautics and Space Administration (NASA)'s Soil Moisture Active Passive (SMAP) mission provides reliable global observations of surface soil moisture; however, several limitations reduce its suitability for field-scale agricultural applications [21] [22]. SMAP's spatial resolution (~9 - 36 km) is too coarse to capture farm-level variabilities or to support pixel-level comparison with point-based field soil sensors [23]. The SMAP data product also directly captures moisture dynamics at the upper 5 cm of the soil profile. SMAP, however, provides additional "root-zone" soil moisture products generated through land-surface model assimilation rather than direct measurements. This limits the suitability for validating subsurface moisture at specific depths [11]. Some of these constraints highlight the value of multispectral systems such as Landsat 8/9 and Sentinel-2, which provide freely accessible imagery with 10 - 30 m spatial resolution and spectral bands sensitive to vegetation water content [24]-[26]. Numerous studies have explored a range of spectral indices for drought monitoring and moisture assessment. The use of these indices, such as Land Surface Temperature (LST), Normalized Difference Vegetative Index (NDVI), Normalized Temperature Drought Index (NTDI), Normalized Difference Water Index (NDWI), Normalized Soil Moisture Index (NSMI), Modified Perpendicular Drought Index (MPDI) has shown the effectiveness of satellite data to analyze soil and vegetation moisture conditions [27]-[31].

Comprehensive reviews further indicate that vegetation indices derived from multispectral imagery are often incorporated into statistical and machine-learning frameworks for soil moisture estimation. However, most prior studies focus on surface soil moisture products or aggregated root-zone estimates [32]. This highlights the need for depth-specific assessment of vegetative moisture signals within field-scale agricultural systems. Among these commonly applied indices, the Normalized Difference Moisture Index (NDMI) and Moisture Stress Index (MSI) are particularly relevant because they rely on direct NIR-SWIR relationships that are physically sensitive to plant and canopy water content [33] [34]. NDMI reflects

vegetation water abundance, while MSI increases with moisture deficit and canopy stress. Since vegetation moisture integrates short-term rainfall, soil hydraulic conditions, and plant uptake, canopy-based indices may reflect soil moisture dynamics at different depths.

Despite these advancements, significant limitations remain in estimating soil moisture at root-zone depths using remote sensing [35] [36]. The reliability of satellite-based soil moisture products can be reduced by vegetation types, atmospheric effects, and variability in soil texture and structure, particularly in heterogeneous agricultural systems [37]-[39]. Most existing studies evaluate remote sensing indices against surface soil moisture or at single-depth measurements, leaving a limited understanding of how index-moisture relationships vary across root-zone depths. Yet this depth-specific evaluation is critical for irrigation scheduling, since crop water uptake is concentrated within root zone layers [40]. To optimize irrigation, understanding depth-resolved soil moisture dynamics is essential. Accordingly, there is a need to evaluate how satellite data-based moisture indices relate to soil moisture at multiple depths, especially during the active growing season. This study addresses that gap by assessing the statistical relationships between Landsat- and Sentinel-derived moisture indices and *in-situ* soil moisture measurements at four depths (15, 20, 25, and 30 cm) across agricultural sites in the Alabama Black Belt Region of the Southeastern United States. Specifically, the research objectives are to: 1) develop moisture indices (NDMI and MSI) from Landsat 8/9 and Sentinel-2 imagery and quantify their relationships with multi-depth *in-situ* moisture measurements across the study locations; 2) identify the soil depth(s) at which satellite indices exhibit the strongest correlation with ground truth *in-situ* soil moisture measurements, thereby identifying the optimal depth range for satellite-based soil moisture estimation. In selecting NDMI and MSI, this study prioritizes indices that incorporate NIR-SWIR band combinations sensitive to vegetation water absorption features. These indices rely on spectral bands that are consistently available across Landsat 8/9 and Sentinel-2 platforms. The research enhances knowledge of soil moisture modeling and estimation, which is critical for supporting irrigation planning and water use efficiency across farming systems.

2. Materials and Methods

2.1. Study Area

This research was conducted across five research farms located in Macon, Dallas, and Perry Counties within the Alabama Black Belt Region (ABBR) (**Figure 1**). The ABBR is a diverse region with rich agricultural land within the state of Alabama. The region forms part of the historical Black Belt Region of the southeastern United States [41] [42].

The geographic region for ABBR encompasses 18 counties in central Alabama, including Sumter, Greene, Hale, Marengo, Choctaw, Perry, Dallas, Wilcox, Lowndes, Butler, Crenshaw, Montgomery, Pike, Bullock, Macon, Barbour, Pickens, and Rus-

sell. A significant geological feature of the ABBR is the Selma Chalk (Rotten limestone), a specific formation within the Selma Group [43] [44]. The Selma Chalk, composed primarily of marl and chalk, was deposited during the Late Cretaceous period and is particularly prominent in the ABBR [45] [46]. It serves as a foundation for the region's calcareous, sediment-rich, fertile, dark soils, which support the cultivation of row and specialty crops such as cotton, wheat, corn, and vegetables, especially with irrigation, where feasible [42]. While most of the soils in the State of Alabama belong to the Ultisols soil order group, diverse soil textures are found in the research counties, including loams, sandy loams, silt loams, and sandy clay loams [46]. These counties have diverse soil characteristics and are of agricultural significance to the ABBR [34].

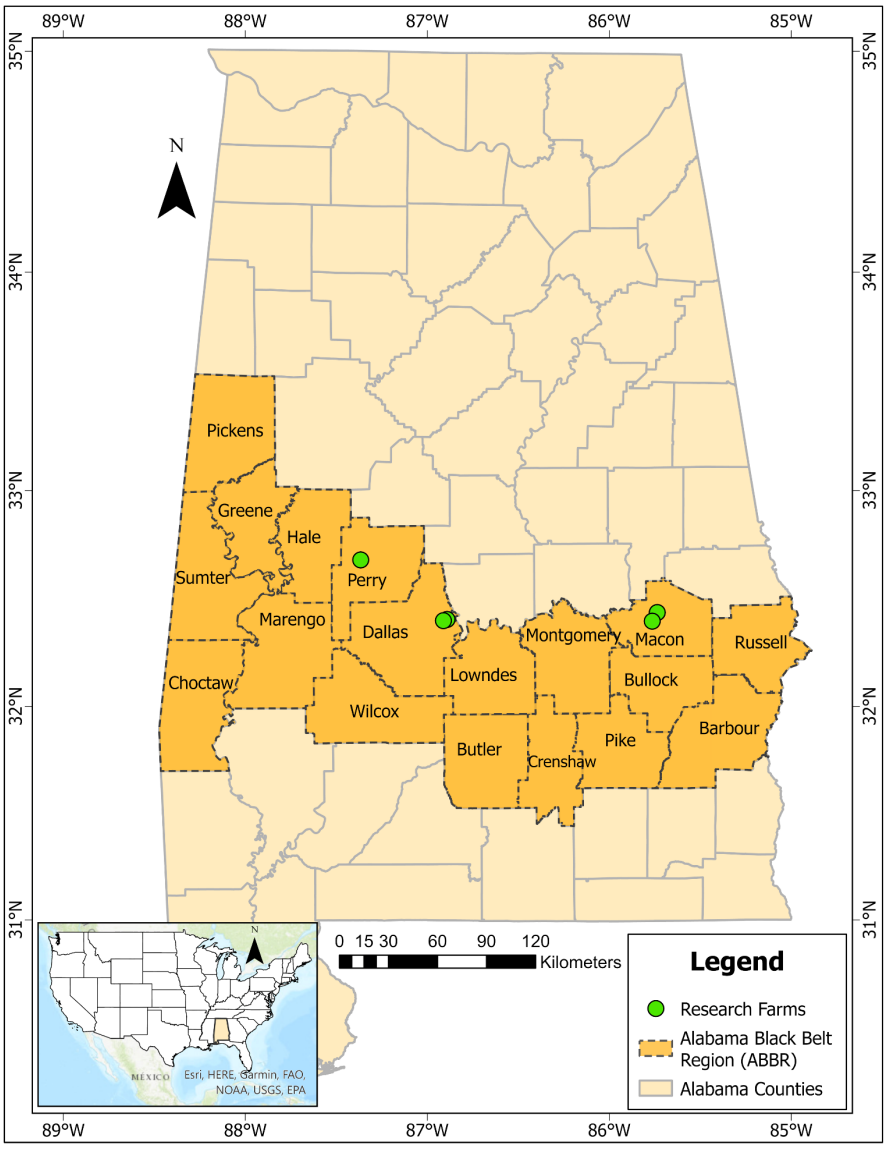

Figure 1. Study area showing ABBR counties and *in-situ* sensor data logger research farm locations.

2.2. Soil Sensor Deployment

In July of 2023, twenty TEROS 12 soil sensors and five ZL6 cellular data loggers, accessible via the ZENTRA cloud, were installed in 5 specialty crop farmers' fields in Dallas, Perry, and Macon counties within the ABBR (Table 1). Each data logger was wired to four soil sensors, each measuring soil volumetric water content (VWC), temperature, and bulk electrical conductivity (EC) at varying depths of 15 cm, 20 cm, 25 cm, and 30 cm. Data loggers 1 and 2 were located in Macon County, data loggers 3 and 4 in Dallas County, and data logger 5 in Perry County. Since July 2023, these sensors have provided real-time measurements of soil conditions, providing over two years of records spanning multiple weather conditions, rainfall events, and crop growing seasons. The spatial distribution of sensors across three counties and five farms was designed to sample soil conditions for contrasting soil and agricultural management practices while still enabling cross-site comparison. Table 1 summarizes the data logger IDs, farm names, coordinates, elevation, county, and installation start times.

Table 1. Information on *in-situ* soil sensor data loggers.

Data Logger ID	Sensor locations	Latitude	Longitude	Elevation (m)	County	Collection Start Date/Time
1	TUOrg_Farm	32.43631	−85.7367	123	Macon	13-07-23 16:22
2	Blueberry	32.39624	−85.7642	111	Macon	24-07-23 15:00
3	BrownDallas	32.40365	−86.8916	45	Dallas	12-08-23 12:22
4	SmithDallas	32.39807	−86.9112	43	Dallas	08-08-23 12:07
5	MurphyPerry	32.67967	−87.3657	128	Perry	08-08-23 14:52

2.3. Satellite Data Preprocessing

Satellite imagery was acquired from August 2023 to October 2025, coinciding with the *in-situ* sensor monitoring period. This window covers two agricultural growing seasons for most crops in Alabama (April-October), allowing the analysis to focus on periods when vegetation is active [47] [48]. Although harmonized multi-sensor products such as NASA's Harmonized Landsat-Sentinel (HLS) dataset are available [49] [50], this research intentionally used native Landsat 8/9 Operational Land Imager (OLI) and native Sentinel-2 Multispectral Instrument surface reflectance products as separate datasets to evaluate how each sensor individually captures soil moisture variability at the *in-situ* sites. Landsat 8/9 and Sentinel-2 imagery were obtained through Google Earth Engine (GEE), which provides cloud-based access to the official U.S. Geological Survey (USGS) and Copernicus/ESA surface reflectance archives [51]. The study used three collections: LANDSAT/LC08/C02/T1_L2, LANDSAT/LC09/C02/T1_L2, and COPERNICUS/S2_SR_HARMONIZED [52]. GEE distributes these datasets in their native formats, preserving the USGS Landsat Collection 2 Level-2 surface reflectance pre-processing and the

ESA Level-2A atmospheric correction applied to Sentinel-2 imagery [53]-[55].

Landsat 8 and 9 provide data with 30m spatial resolution and 16-day temporal resolution, with a combined temporal resolution of approximately 8 days between the two. Sentinel-2 Level-2A imagery offers 10 - 20 m spatial resolution with a roughly 5-day revisit time over the study area [53]-[55]. These datasets provide the spectral configuration needed to compute moisture indices and align satellite overpasses with study counties and field sensors. County boundaries for Macon, Dallas, and Perry were used as spatial filters within GEE to ensure that only scenes intersecting the study area were queried. This filtering minimized unnecessary data downloads and facilitated temporal alignment with the *in-situ* sensor record. For each retained scene, key metadata, which includes acquisition date, cloud statistics, scene identifiers, and Landsat WRS Path/Row, were exported for subsequent cloud-threshold analysis and scene selection. For Sentinel-2, the S2_SR_HARMONIZED collection in GEE ensures that mixed-resolution bands are resampled onto a common grid before export. This internal harmonization prevents spatial misalignment between Band 8 (10 m) and Band 11 (20 m) and ensures consistent pixel-level extraction of pixel values at sensor locations.

All downloaded Landsat and Sentinel scenes were clipped to the exact county boundaries of Macon, Dallas, and Perry using official county shapefiles and projected into a common coordinate system (UTM Zone 16N - EPSG: 32616). The original radio-metric properties of each data set were preserved to avoid smoothing or blending effects that could alter the moisture index-soil moisture relationship. For Landsat 8/9, surface reflectance scaling (Equation (1)) was applied according to the standard USGS Collection 2 transform [53]:

$$\text{Reflectance} = 0.0000275 \times \text{DN} - 0.2 \quad (1)$$

This correction was applied before the index computation to convert digital numbers (DN) to the soil moisture biophysical index product. Sentinel-2 Level-2A (S2_SR_HARMONIZED) is provided directly in a corrected surface reflectance, so no additional scaling of DN values was necessary. Cloud screening was performed using the scene-level cloud metrics provided in the satellite metadata. To assess the influence of cloud contamination on MI-SM relationships, three thresholds (≤15%, ≤10%, and ≤5%) were evaluated. The ≤5% subset was selected for the primary analysis in this study to ensure the highest data quality, while higher thresholds were used during preliminary assessment to evaluate sensitivity to cloud filtering. The overall methodological workflow integrating satellite data processing, *in-situ* soil moisture aggregation, dataset harmonization, and statistical analysis is summarized in **Figure 2**.

2.4. Field Soil Sensor Data

Records of volumetric water content (VWC) at 15-minute intervals for four study depths (15, 20, 25, and 30 cm) at all five research farms were obtained from field soil sensor data loggers via the Zentra cloud platform. Time-series processing and

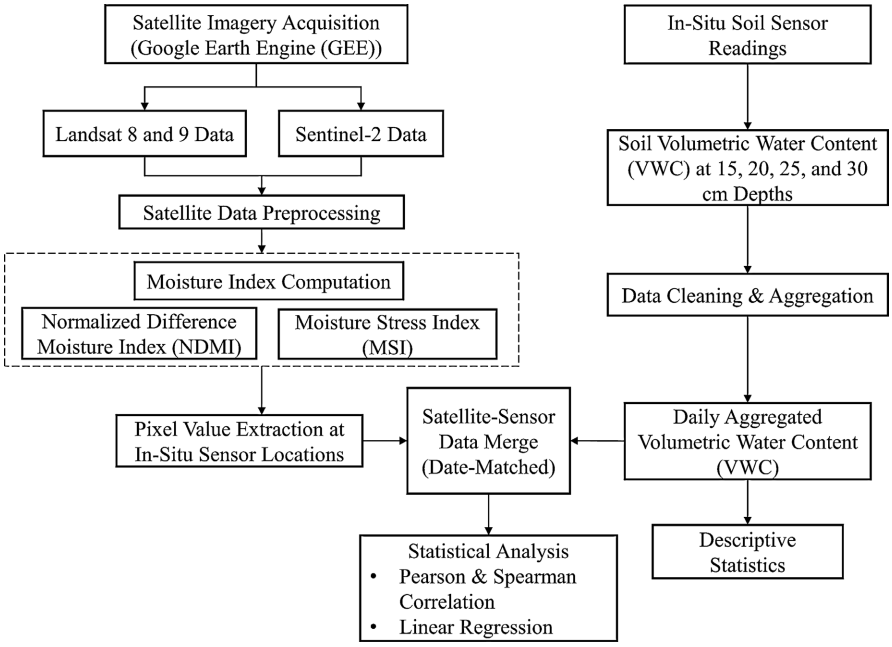

Figure 2. Overview of the methodological workflow integrating *in-situ* soil moisture measurements and satellite-derived moisture indices for statistical analysis.

quality control were conducted before integrating measured soil data with satellite-derived indices. First, the 15-minute readings were aggregated to hourly averages to reduce high-frequency noise. To synchronize with satellite overpass times, daily soil moisture values were aggregated over the 16:00-17:00 UTC window. Satellite acquisition times extracted from scene-level metadata for this study ranged between approximately 16:00 and 16:45 UTC across Landsat 8/9 and Sentinel-2 observations. The selected averaging window was therefore chosen to minimize temporal mismatch between satellite and *in-situ* soil sensor measurements. These aggregated values were used as the *in-situ* VWC and matched to each satellite's acquisition date. In all cases, soil moisture values were matched to the same calendar day as the satellite acquisition, with no temporal shifting applied.

A quality control assessment was conducted using the whole record from August 2023 to October 2025. For each depth, pairwise Pearson correlations were computed across all five sites to evaluate temporal analysis and identify potential sensor anomalies. Cross-site correlations ranged from approximately 0.65 to 0.94, with correlation strength generally increasing with depth. This pattern is consistent with stronger hydraulic buffering and reduced short-term variability in deeper soil layers. No sensor exhibited physically inconsistent behavior over the two years, indicating that the *in-situ* network provided a reliable ground-truth reference for evaluating satellite-derived moisture indices.

Descriptive statistics were also computed from daily VWC measurements from soil sensors, spanning the entire observation period (August 2023 - October 2025). For each site and depth, mean, standard deviation (SD), minimum, maximum, and coefficient of variation (CV) were calculated (Table 2). This revealed variability across the five sites. The statistics characterized site-level soil moisture con-

ditions across seasons and provided contextual information for subsequent statistical analysis. The descriptive statistics were, however, computed independently of satellite acquisition dates to avoid sampling bias.

Table 2. Descriptive statistics of daily volumetric water content (m^3/m^3) at four depths (15-30 cm) across the five study sites for the observation period (August 2023 - October 2025).

Data Logger ID	Depth (cm)	Mean	SD	Minimum	Maximum	CV (%)
1	15	0.289	0.028	0.234	0.350	9.82
	20	0.302	0.024	0.244	0.358	8.04
	25	0.300	0.038	0.214	0.401	12.53
	30	0.215	0.039	0.150	0.292	18.04
2	15	0.157	0.048	0.073	0.397	30.68
	20	0.190	0.064	0.085	0.365	33.45
	25	0.191	0.049	0.098	0.382	25.57
	30	0.191	0.066	0.083	0.354	34.56
3	15	0.147	0.042	0.091	0.352	28.47
	20	0.139	0.040	0.084	0.290	28.59
	25	0.147	0.042	0.092	0.361	28.75
	30	0.143	0.036	0.095	0.283	24.80
4	15	0.174	0.047	0.105	0.343	27.28
	20	0.152	0.043	0.096	0.304	28.23
	25	0.162	0.049	0.100	0.304	30.46
	30	0.147	0.040	0.094	0.300	27.51
5	15	0.218	0.037	0.151	0.374	16.96
	20	0.224	0.039	0.155	0.293	17.45
	25	0.273	0.027	0.218	0.365	9.83
	30	0.293	0.027	0.240	0.330	9.07

2.5. Moisture Index Computation

Moisture indices were computed from the Short-Wave Infrared Band 1 (SWIR1) and Near-Infrared (NIR) bands of Landsat 8/9 and Sentinel-2. For Landsat, Band 5 (NIR) and Band 6 (SWIR1) were used. For Sentinel-2, Band 8 (NIR) and Band 11 (SWIR1) were used, consistent with established practice for NDMI and MSI computation. Sentinel-2 provides NIR (Band 8) at 10 m resolution and SWIR1 (Band 11) at 20 m. When accessed through GEE, Band 8 was resampled to 20 m to ensure pixel alignment with Band 11 during export. This harmonization enables accurate NDMI and MSI calculation from co-registered pixels and introduces only minor smoothing relative to native 10-m NIR data. Because all analyses relied

on point-level pixel extraction at sensor coordinates, the impact of this resampling on index values was negligible. Two moisture-sensitive spectral indices were then calculated for each scene:

- Moisture Stress Index (MSI): The MSI is a spectral index used to quantify water content or stress in vegetation based on spectral reflectance ratios of the moisture-sensitive shortwave infrared (SWIR) and the less-sensitive near-infrared (NIR) bands (Equation (2)). Higher values signify greater moisture stress or less moisture content in vegetation and vice versa for lower values of MSI [34];

$$\mathrm{MSI} = \frac{\mathrm{SWIR}}{\mathrm{NIR}}. \tag{2}$$

- Normalized Difference Moisture Index (NDMI): The NDMI is a biophysical spectral reflectance index used to assess moisture content in vegetation and the broader environment (Equation (3)). High NDMI values indicate high vegetation water content, whereas low values indicate lower water content [56].

$$\mathrm{NDMI} = \frac{\mathrm{NIR} - \mathrm{SWIR}}{\mathrm{NIR} + \mathrm{SWIR}} \tag{3}$$

Index computation was performed in ERDAS IMAGINE, using batch workflows with Python scripts to generate MSI and NDMI for each Landsat and Sentinel scene. After index products were created, pixel values for NDMI and MSI were extracted at the exact coordinates of each data logger location. For each date where satellite imagery and soil moisture readings overlapped, a record was stored containing site ID, county, date, NDMI, MSI, and soil moisture (VWC) at each depth (15, 20, 25, 30 cm). This produced a harmonized dataset for analysis. Following all preprocessing, only dates with valid, non-missing soil moisture data and corresponding NDMI and MSI values were retained. These harmonized records formed the analysis-ready dataset for subsequent correlation and regression.

2.6. Statistical Analysis and Sensor Selection

Statistical analysis was performed to quantify the relationship between satellite-derived moisture indices (NDMI and MSI) and in situ soil moisture at each location and depth. All statistical computations were performed in Python (v3.12) [57], with additional verification in Microsoft Excel to ensure consistency of regression outputs and summary statistics. To characterize these relationships, both Pearson (r) and Spearman correlation (ρ) coefficients were computed between NDMI, MSI, and soil moisture readings at 15, 20, 25, and 30 cm. Pearson correlations captured linear trends (Equation (4)). In contrast, Spearman correlations identified monotonic trends that might persist even when linearity was weaker. Spearman's correlation coefficient evaluates the strength of association based on the rank ordering of paired moisture index and soil moisture (MI-SM) values (Equation (5)), which can be informative when the MI-SM relationship is affected by local heterogeneity or non-linear trends [58] [59]. Initial correlations were computed using all twenty *in-situ* soil sensors (IDs 1-5) to provide a regional per-

spective on depth-specific behavior. Pearson and Spearman coefficients were calculated using the following standard formulas in Equations (4) and (5) [57] [59]:

$$\text{Pearson correlation } (r) = \frac{\sum_{i=1}^{n}\left(x_i-\overline{x}\right)\left(y_i-\overline{y}\right)}{\sqrt{\left[\sum_{i=1}^{n}\left(x_i-\overline{x}\right)^2\right]\left[\sum_{i=1}^{n}\left(y_i-\overline{y}\right)^2\right]}} \quad (4)$$

$$\text{Spearman rank correlation } (\rho) = 1-\frac{6\sum_{i=1}^{n}d_i^2}{n\left(n^2-1\right)} \quad (5)$$

where n is the sample size, x is the independent variable, and y is the dependent variable, and d_i is the difference between the ranks of paired observations.

For a refined regression modeling, one representative site was selected from each county to maintain balanced geographic coverage across Macon, Dallas, and Perry Counties (Data Logger IDs 1, 4, 5). Selection criteria included 1) sufficient paired observations after harmonization and ≤5% cloud filtering across both Landsat 8/9 and Sentinel-2 to support stable statistical analysis, and 2) consistent and lower site-level variability in soil moisture behavior across depths (**Table 2**), during the initial screening analysis. This approach preserved regional representation while focusing on sites exhibiting stable vertical moisture structure. Site-level differences in soil and crop conditions were acknowledged as potential influences on MI-SM relationships. To evaluate predictive accuracy, simple linear regression models (Equation (6)) were fitted separately for each satellite, index, and depth combination:

$$\text{Soil Moisture} = (a \times \text{Index}) + b. \quad (6)$$

where a - is the regression slope representing the rate of change in soil moisture per unit change in the satellite moisture index, and b is the intercept representing the predicted soil moisture value when the index is zero.

For each model, slope, intercept, Pearson r, coefficient of determination (r^2), p-value, standard error, and root-mean-square error (RMSE) were extracted to assess statistical significance and model performance. After applying the preprocessing and harmonization steps, paired satellite-sensor datasets for Landsat 8/9 and Sentinel-2 spanning August 2023 to October 2025 during the growing season were obtained. Paired observation counts after harmonization and filtering were summarized by county and satellite (**Table 3**). Counts represent aggregated observations across data loggers within each county. Because each satellite observation was matched with soil moisture measurements at all four depths, counts were

Table 3. Summary of paired observation counts (n) by county and satellite following harmonization and filtering.

County	Landsat n (per depth)	Sentinel n (per depth)
Macon	66	36
Dallas	32	40
Perry	31	17

consistent across depths within each county. Across all datasets, MSI values ranged from 0.5 to 1.5, while NDMI values typically spanned −0.2 to 0.25, reflecting expected stress-to-moisture gradients within the canopy.

3. Results

3.1. Overview of MI-SM Relationship

Initial correlation across all twenty *in-situ* sensors within the research counties established a baseline before a refined analysis. Across all sensors, a consistent depth-dependent structure emerged. For Landsat 8/9, correlations were weak at shallow layers (15 - 20 cm), with NDMI producing $r \approx 0.13$ at 15 cm and $r \approx 0.18$ at 20 cm. At 25 cm, correlations strengthened (NDMI $r \approx 0.34$), while the strongest relationships occurred at 30 cm (NDMI $r \approx 0.47$; MSI $r \approx -0.45$). Sentinel-2 exhibited a similar depth-dependent structure but with stronger overall associations. At 15 cm, NDMI produced $r \approx 0.34$, increasing to $r \approx 0.44$ at 20 cm and reaching $r \approx 0.50$ - 0.53 at 25 - 30 cm depths. MSI exhibited negative correlations with NDMI, consistent with its stress-based formulation, in which higher MSI values indicate greater moisture stress and, therefore, lower soil moisture. Across both sensors, MI-SM coupling strengthened with increasing depth, with deeper layers exhibiting the most stable relationships. To further examine site-level structure while maintaining balanced geographic coverage, a representative subset of one site per county was analyzed in greater detail. This refinement preserved the depth-dependent pattern observed across the whole dataset and enabled a more precise evaluation of MI-SM behavior.

3.1.1. Landsat 8/9

Landsat 8/9 exhibited a clear depth-dependent pattern in MI-SM coupling, within the refined subset (Table 4). The performance improves from shallow layers (15 - 20 cm) to 30 cm depth (Table 4). Under the strictest cloud condition threshold (≤5%, n = 80), NDMI at 15 cm produced $r \approx 0.11$, while MSI yielded $r \approx -0.12$.

Table 4. Pearson and Spearman correlations between Landsat 8/9 indices and *in-situ* soil moisture.

Satellite-Index	Depth (cm)	n	Pearson (r)	Spearman (ρ)
Landsat 8/9 - NDMI	15	80	0.114	0.096
	20	80	0.161	0.149
	25	80	0.425	0.335
	30	80	0.624	0.615
Landsat 8/9 - MSI	15	80	−0.119	−0.096
	20	80	−0.168	−0.149
	25	80	−0.427	−0.335
	30	80	−0.635	−0.615

Correlations increased only slightly at 20 cm (NDMI r ≈ 0.16; MSI r ≈ −0.17), while NDMI at 25 cm achieved r ≈ 0.43, with MSI showing r ≈ −0.43. At 30 cm, Landsat reached its highest correlations, with NDMI r ≈ 0.62 and MSI r ≈ −0.64. Results indicate poor correlations between NDMI and MSI and soil moisture at shallow soil layers/depths, whereas the strongest correlations occur at 30 cm depth. However, the Pearson and Spearman coefficients were almost identical at each depth, reinforcing that Landsat's MI-SM relationships were predominantly linear.

3.1.2. Sentinel-2

Sentinel-2 also exhibited a depth-dependent correlation with soil moisture, however, with stronger overall MI-SM relationships than Landsat, especially at shallow and mid-depth levels (Table 5). Under the strictest cloud condition threshold (≤5%, n = 73), Sentinel correlation had NDMI r ≈ 0.49 and MSI r ≈ −0.48 at 15 cm depth, while that for 20 cm was NDMI r ≈ 0.51 and MSI r ≈ −0.50. These values are higher compared to Landsat, and indicate moderate MI-SM relationships, with Spearman coefficients ($\rho \approx 0.54$ - 0.55) consistently exceeding Pearson r. At depths of 25 - 30 cm, the strongest Sentinel-2 MI-SM relationships occurred, where NDMI correlations ranged from r ≈ 0.60 to 0.61, with MSI exhibiting similar values in the opposite direction. Overall, Sentinel-2 maintained robust MI-SM relationships for mid- and deep-layer (25 - 30) soil moisture.

A notable pattern, however, emerged: Spearman correlations for Sentinel-2 were consistently slightly higher than the corresponding Pearson values for all depth levels. This suggests a strong monotonic MI-SM relationship even when linearity was less pronounced.

Table 5. Pearson and Spearman correlations between Sentinel 2 indices and *in-situ* soil moisture.

Satellite-Index	Depth(cm)	n	Pearson (r)	Spearman (ρ)
Sentinel 2 - NDMI	15	73	0.490	0.541
	20	73	0.513	0.554
	25	73	0.611	0.652
	30	73	0.600	0.595
Sentinel 2 - MSI	15	73	−0.478	−0.541
	20	73	−0.503	−0.554
	25	73	−0.603	−0.652
	30	73	−0.598	−0.595

3.2. Comparative Performance NDMI and MSI

NDMI and MSI provided biophysical indications of vegetation and soil moisture status. NDMI increases as vegetation and soil moisture levels increase. On the other hand, MSI increases with increasing moisture stress and decreasing soil moisture levels. Across all satellite data types and depths, the two indices per-

formed similarly, with only minor differences in correlation strength. For Landsat 8/9, MSI consistently produced slightly stronger absolute correlations than NDMI at all depths, although the advantage was slight (typically 0.005 - 0.01 in |r|). At 30 cm, where Landsat performed best, both indices reached nearly identical strengths (|r| ≈ 0.60 - 0.64). Despite these differences, both indices followed the same depth pattern: weak relationships at 15 - 20 cm, stronger sensitivity at 25 cm, and the most stable indicator at 30 cm. This consistency indicates that NDMI and MSI are essentially interchangeable for soil-moisture estimation in this landscape, with neither index showing a clear systematic advantage. To illustrate their spatial behavior, Figures 3-6 present MSI and NDMI maps for September 2025 conditions across Macon, Dallas, and Perry counties, highlighting county-level variations in

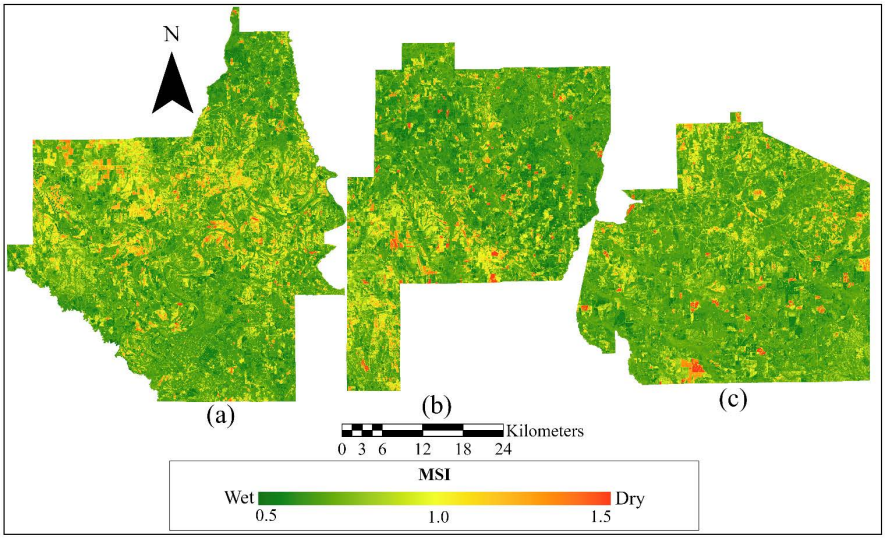

Figure 3. MSI-based Moisture maps for Dallas (a), Perry (b), and Macon (c) counties for September 2025, derived from Landsat 9.

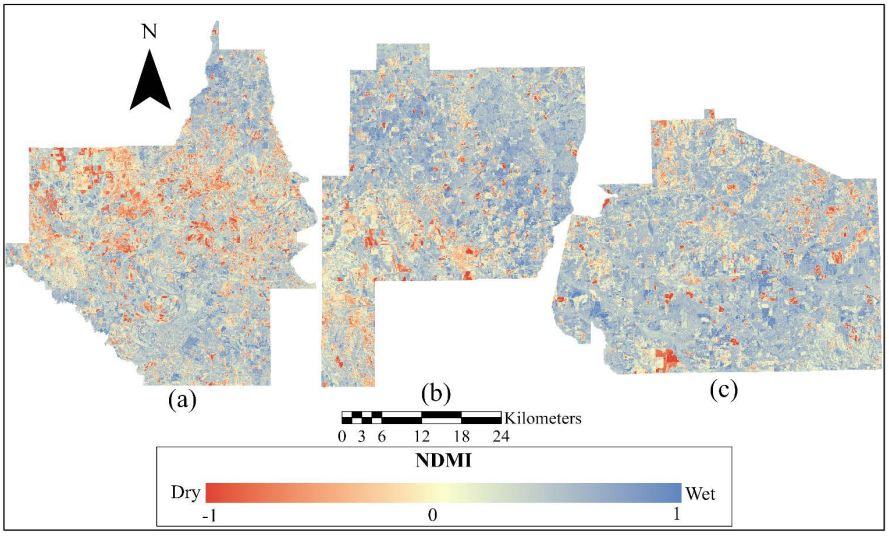

Figure 4. NDMI-based moisture maps for Dallas (a), Perry (b), and Macon (c) counties for September 2025, derived from Landsat 9.

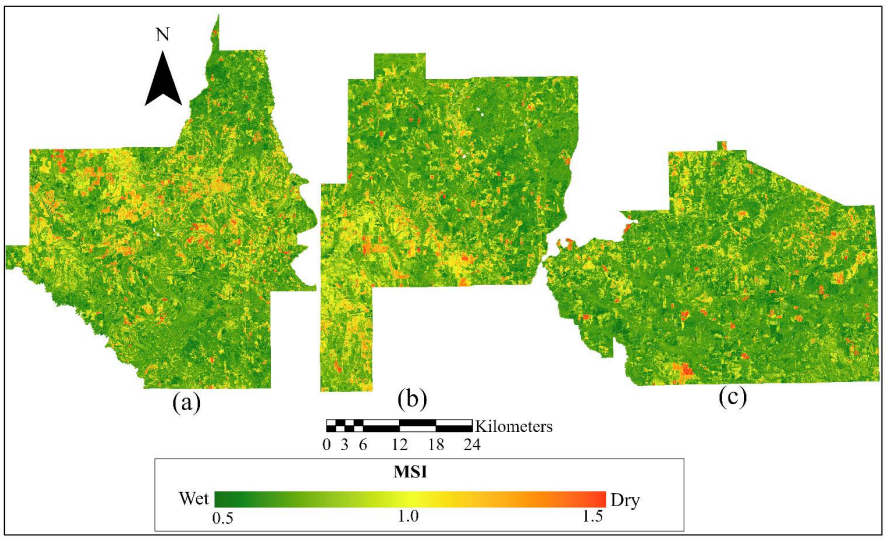

Figure 5. MSI-based moisture maps for Dallas (a), Perry (b), and Macon (c) counties for September 2025, derived from Sentinel 2.

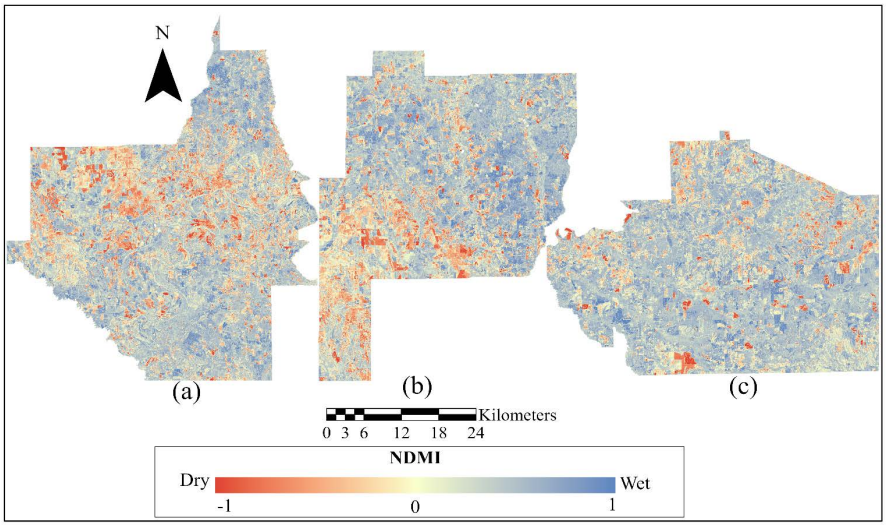

Figure 6. NDMI-based Moisture maps for Dallas (a), Perry (b), and Macon (c) counties for September 2025, derived from Sentinel 2.

vegetation moisture conditions during the growing season. The maps show that moisture conditions are not uniform across counties. Some areas appear drier (with higher MSI and lower NDMI values), while others seem relatively wetter. NDMI and MSI also display inverse spatial patterns, consistent with their physical formulation. The Sentinel-2 maps (**Figure 5** and **Figure 6**) also show slightly finer spatial detail, consistent with its higher spatial resolution. Any preference for one index over the other should therefore be guided more by conceptual framing (moisture or stress emphasis) and modeling choices.

3.3. Regression Analysis

Regression modeling was further used to assess the relative strength of the MI-

SM relationships across Landsat 8/9 and Sentinel-2, at different soil depths. Separate linear models were fitted for each index (Table 6), and both indices produced statistically significant regressions ($p < 0.01$). For Landsat 8/9, NDMI and MSI both produced strong and statistically significant regressions at 30 cm depth, with the lowest RMSE values among all regressions, indicating that Landsat can provide highly accurate linear predictions of soil moisture at this depth. For Sentinel, the slightly lower RMSE value at 30 cm compared to 25 cm suggests tighter coupling between Sentinel indices and Soil moisture at deeper depths. Scatterplots with fitted lines (Figures 7(a)-(d)) reinforce these results, showing

Table 6. Regression performance for MI-SM relationships across Landsat 8/9 and Sentinel-2.

Satellite	Depth	Index	n	r	r^2	RMSE (m^3/m^3)
Landsat 8/9	30 cm	NDMI	80	0.624	0.389	0.0495
Landsat 8/9	30 cm	MSI	80	−0.635	0.404	0.0489
Sentinel-2	30 cm	NDMI	73	0.600	0.360	0.0554
Sentinel-2	30 cm	MSI	73	−0.598	0.358	0.0555
Sentinel-2	25 cm	NDMI	73	0.611	0.373	0.0637
Sentinel-2	25 cm	MSI	73	−0.603	0.363	0.0642

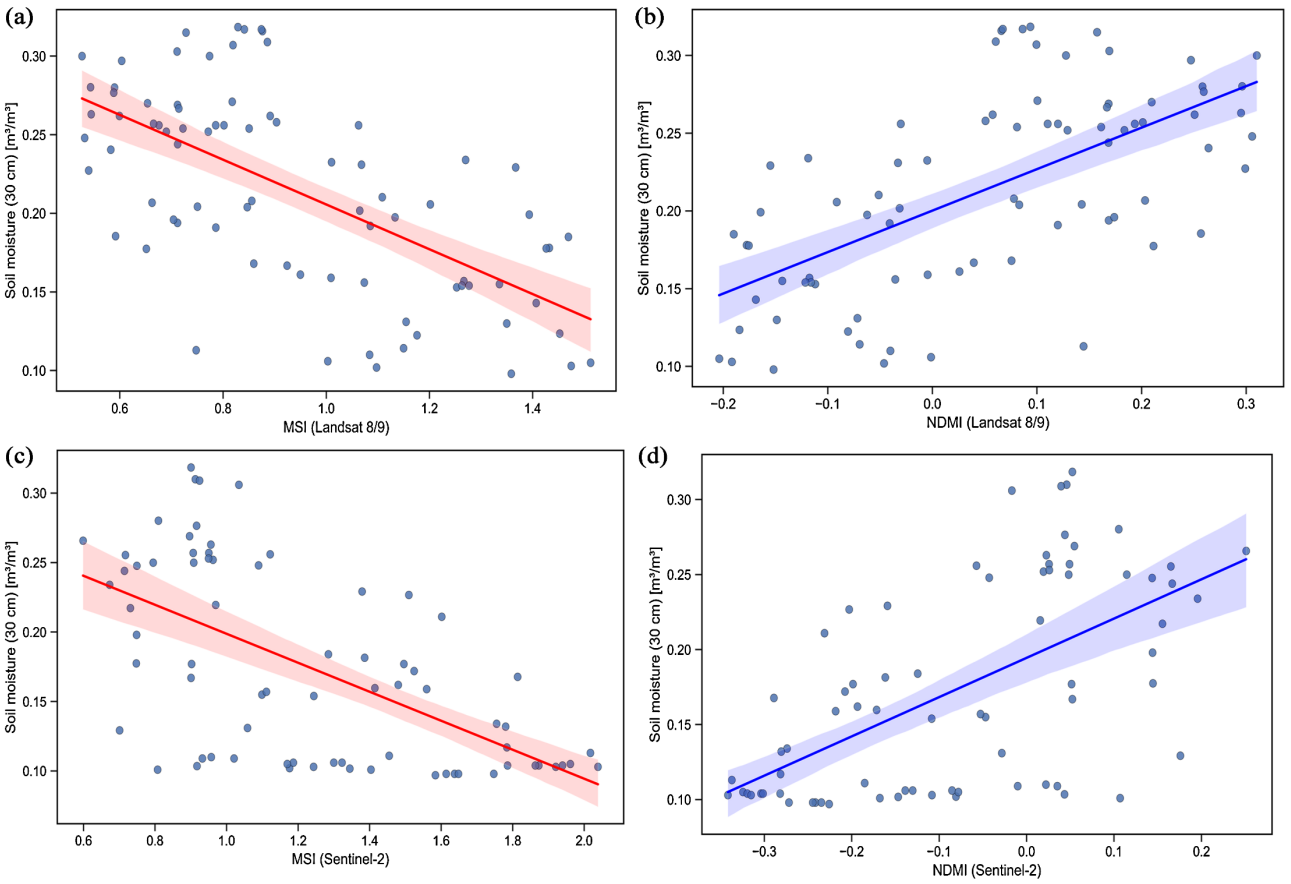

Figure 7. MI-SM scatterplots with fitted linear regression lines for 30 cm soil depth for Landsat 8/9 (a) MSI; (b) NDMI and Sentinel-2 (c) MSI; (d) NDMI.

clear MI-SM linear relationships at 30 cm depth.

4. Discussion

This research evaluated how satellite-derived moisture indices capture soil moisture variability across four depths during the active growing seasons of 2023-2025 in the Alabama Black Belt Region. Across satellites, indices, and depths, a consistent pattern emerged. Depth is the dominant control on MI-SM strength. Relationships are weak at 15 - 20 cm, but strengthened at 25 - 30 cm. This holds for both Landsat and Sentinel and across NDMI and MSI. This depth-dependent behavior reflects the fact that deeper soil layers exhibit greater soil moisture stability and may strengthen statistical associations between canopy-based spectral indices and subsurface moisture conditions. The slopes of MSI and NDMI align with theoretical expectations: increasing MSI or decreasing NDMI indicates reduced vegetation moisture, which corresponds to lower soil moisture. All regression models at 25 - 30 cm were statistically significant ($p < 0.01$), indicating that the observed relationships are unlikely to be due to random variability. However, because NDMI and MSI are derived from surface reflectance, their correlation with deeper soil layers should be interpreted as indirect. Stronger correlations at 25 - 30 cm may also arise from hydraulic connectivity across depths. In addition, this depth range corresponds more closely to the active root-zone for many crops, where plant water uptake is most stable. Soil texture and infiltration dynamics may also contribute to moisture retention at these deeper depths. These factors can lead to more stable moisture conditions, as reflected in the canopy water status.

It is also important to acknowledge the spatial scale differences between satellite pixel resolutions (30 m for Landsat 8/9 and 20 m for Sentinel-2) and the point-based *in-situ* soil moisture sensors. Variability in soil texture, micro-topography, and localized management practices within a single pixel may introduce heterogeneity that is not fully captured by the sensor footprint. Consequently, the reported correlations reflect aggregated canopy responses at the pixel scale, which may influence the strength of MI-SM relationships.

A comparatively stronger shallow-layer relationship was also observed in Sentinel-2 analysis relative to Landsat. Differences in sensor configurations between these two systems may partially explain this. Sentinel-2's finer spatial resolution relative to Landsat may reduce sub-pixel heterogeneity effects, potentially enhancing the detection of localized vegetation moisture variability [26]. Although the effect remains context-dependent, the spatial, spectral, and sensor design differences provide a basis for the observed cross-sensor variability. Beyond these differences, the results confirm that integrating Landsat and Sentinel imagery can increase the frequency of observations, thereby improving the ability to track moisture conditions throughout the growing season.

The results confirm that each index provides unique, yet complementary, information for analyzing spatiotemporal trends in soil moisture. Together, the indices provide a more comprehensive representation of moisture dynamics. Their

parallel performance across depths suggests that both products contribute to satellite-based moisture estimation in agricultural ecosystems. Both indices demonstrated consistent depth-dependent patterns, indicating utility for monitoring moisture variability under agricultural conditions, even when subsurface moisture cannot be directly observed. Each could, however, be used in the context of water stress or vegetative moisture conditions. The findings directly address the identified gap concerning the limited evaluation of depth-dependent satellite-subsurface moisture coupling in agricultural systems. By assessing multiple farms and two satellite platforms over consecutive growing seasons, this study clarifies how moisture indices relate to soil moisture variability within the 15 - 30 cm profile. Overall, these results show that NDMI and MSI serve as effective indirect indicators of subsurface moisture, though their performance can be influenced by canopy structure, vegetation type, and soil properties [60].

This study also intentionally restricted modeling to three representative data logger locations with twelve sensors that exhibited stable MI-SM behavior and spatial coverage. As explained in section 3.1, the full five-site analysis showed the same depth-dependent pattern, with weaker relationships at 15 - 20 cm and stronger relationships at 25 - 30 cm, while the refined subset yielded moderately stronger correlations due to reduced site-level variability. The refined site selection and improved MI-SM consistency further suggest that soil texture variability, hydraulic properties, and localized management practices may influence the strength of satellite-subsurface moisture coupling. Differences in infiltration capacity, rooting depth distribution, and irrigation management can modify how canopy water status responds to subsurface moisture availability. Although these factors were not explicitly modeled in this study, their potential influence highlights the importance of integrating soil physical characteristics and management context into future satellite-based soil moisture assessments. Additionally, crop type is also relevant for interpreting these relationships; this study did not analyze stage-specific dynamics or crop phenological stages. The present study evaluated seasonal correlations at an aggregated level across the growing periods. Incorporating soil, management, and phenological variables into future models could enhance the predictive power of satellite-based soil moisture estimates.

The linear regression models were applied across the study period to characterize the strength of the MI-SM relationship rather than to develop predictive models. No independent temporal validation split was implemented; therefore, the linear formulation may not capture nonlinear soil-plant-atmosphere interactions during transitional wetting and drying cycles. Also, the paired satellite-sensor observations represent repeated measurements from the same locations over time. As a result, observations may not be fully independent. Future work involving mixed-effects approaches is therefore suggested. In addition to modeling limitations, measurement uncertainty should be acknowledged when interpreting MI-SM relationships. The *in-situ* soil moisture sensors used in this study have a manufacturer-reported VWC accuracy of approximately ±0.03 m^3/m^3 [61]. Landsat 8

reflectance calibration uncertainty has been reported at approximately 2%, with radiance calibration uncertainty near 3% [62]. Sentinel-2 Level-2A surface reflectance products are validated against mission performance requirements, with bottom-of-atmosphere reflectance uncertainty defined as $U(\rho) \leq 0.05\rho + 0.005U$ [63]. Overall, the depth pattern in our results, where 30 cm consistency showed the most stable MI-SM relationship, suggests the need for further work on remote sensing-based estimation of soil moisture at deeper depths.

5. Conclusions

This research demonstrates that satellite-based moisture indices exhibit statistically significant, depth-dependent associations with *in-situ* soil moisture during the growing season under low-cloud conditions. Both Sentinel-2- and Landsat-8/9-based moisture indices showed strong statistical correlations at 30 cm with *in-situ* measurements, establishing NDMI and MSI as practical, cost-effective, and efficient means for root-zone moisture estimation. The strengthening of MI-SM relationships with increasing depth suggests that canopy-based spectral indices may be responding to moisture conditions in deeper soil layers rather than reflecting only short-term near-surface variability. The regression relationships serve as a baseline for future predictive tools, which include machine-learning models, harmonized datasets, and operational soil moisture forecasting systems. Because the analysis focused on periods of active vegetation, the resulting relationships reflect meaningful plant-soil interactions relevant for irrigation scheduling and crop water management. Extending the analysis beyond the growing season and integrating site-specific variables will further enhance the applicability of satellite-based soil moisture estimation in agricultural decision support. Together, these results improve the understanding of how moisture indices behave across soil depths and satellite platforms. These advancements will support the development of operational soil moisture prediction tools, enabling more informed irrigation management in regions with limited sensor coverage.

Funding

This research was supported by the Cooperative Institute for Research to Operations in Hydrology (CIROH) with funding under award NA22NWS4320003 from the NOAA Cooperative Institute Program. The statements, findings, conclusions, and recommendations are those of the author(s) and do not necessarily reflect the opinions of NOAA.

Conflicts of Interest

The authors declare no conflicts of interest regarding the publication of this paper.

References

[1] Li, G., Long, H., Zhang, R., Drohan, P.J., Xu, A. and Niu, L. (2023) Stable Soil Moisture Alleviates Water Stress and Improves Morphogenesis of Tomato Seedlings. *Hor-*

ticulturae, **9**, Article 391. https://doi.org/10.3390/horticulturae9030391

[2] Plett, D.C., Ranathunge, K., Melino, V.J., Kuya, N., Uga, Y. and Kronzucker, H.J. (2020) The Intersection of Nitrogen Nutrition and Water Use in Plants: New Paths toward Improved Crop Productivity. *Journal of Experimental Botany*, **71**, 4452-4468. https://doi.org/10.1093/jxb/eraa049

[3] Wang, C., Fu, B., Zhang, L. and Xu, Z. (2019) Soil Moisture-Plant Interactions: An Ecohydrological Review. *Journal of Soils and Sediments*, **19**, 1-9. https://doi.org/10.1007/s11368-018-2167-0

[4] Bodner, G., Nakhforoosh, A. and Kaul, H. (2015) Management of Crop Water under Drought: A Review. *Agronomy for Sustainable Development*, **35**, 401-442. https://doi.org/10.1007/s13593-015-0283-4

[5] Camporese, M., Gumiere, S.J., Putti, M. and Botter, G. (2021) Efficient Irrigation of Maize through Soil Moisture Monitoring and Modeling. *Frontiers in Water*, **3**, Article 627551. https://doi.org/10.3389/frwa.2021.627551

[6] Ahmad, L., Shanono, N.J. and Nasidi, N.M. (2022) Toward Adoption of Drip Irrigation and Soil-Moisture Sensors by Small-Scale Farmers. *FUDMA Journal of Sciences*, **6**, 259-270. https://doi.org/10.33003/fjs-2022-0603-961

[7] Berthold, T.A., Ajaz, A., Olsovsky, T. and Kathuria, D. (2021) Identifying Barriers to Adoption of Irrigation Scheduling Tools in Rio Grande Basin. *Smart Agricultural Technology*, **1**, Article 100016. https://doi.org/10.1016/j.atech.2021.100016

[8] Ganjegunte, G. and Clark, J. (2017) Improved Irrigation Scheduling for Freshwater Conservation in the Desert Southwest U.S. *Irrigation Science*, **35**, 315-326. https://doi.org/10.1007/s00271-017-0546-8

[9] Quiring, S.M., Ford, T.W., Wang, J.K., Khong, A., Harris, E., Lindgren, T., *et al.* (2016) The North American Soil Moisture Database: Development and Applications. *Bulletin of the American Meteorological Society*, **97**, 1441-1459. https://doi.org/10.1175/bams-d-13-00263.1

[10] Kukal, M.S., Irmak, S. and Sharma, K. (2020) Development and Application of a Performance and Operational Feasibility Guide to Facilitate Adoption of Soil Moisture Sensors. *Sustainability*, **12**, Article 321. https://doi.org/10.3390/su12010321

[11] Liu, Y. and Yang, Y. (2022) Advances in the Quality of Global Soil Moisture Products: A Review. *Remote Sensing*, **14**, Article 3741. https://doi.org/10.3390/rs14153741

[12] Schwamback, D., Persson, M., Berndtsson, R., Bertotto, L.E., Kobayashi, A.N.A. and Wendland, E.C. (2023) Automated Low-Cost Soil Moisture Sensors: Trade-Off between Cost and Accuracy. *Sensors*, **23**, Article 2451. https://doi.org/10.3390/s23052451

[13] Sui, R. (2017) Irrigation Scheduling Using Soil Moisture Sensors. *Journal of Agricultural Science*, **10**, Article 1. https://doi.org/10.5539/jas.v10n1p1

[14] Sahaar, S.A. and Niemann, J.D. (2024) Estimating Rootzone Soil Moisture by Fusing Multiple Remote Sensing Products with Machine Learning. *Remote Sensing*, **16**, Article 3699. https://doi.org/10.3390/rs16193699

[15] Wang, Y., Zhao, J., Guo, Z., Yang, H. and Li, N. (2023) Soil Moisture Inversion Based on Data Augmentation Method Using Multi-Source Remote Sensing Data. *Remote Sensing*, **15**, Article 1899. https://doi.org/10.3390/rs15071899

[16] Xuan Wai, M.H., Huong, A. and Ngu, X. (2021) Soil Moisture Level Prediction Using Optical Technique and Artificial Neural Network. *International Journal of Electrical and Computer Engineering*, **11**, Article 1752. https://doi.org/10.11591/ijece.v11i2.pp1752-1760

[17] Zavala Díaz, N.A., Olivares-Rojas, J.C., Zavala Díaz, J., Reyes Archundia, E., Téllez Anguiano, A.D.C., Chávez Campos, G.M., *et al.* (2024) Study of Machine Learning Techniques for the Estimation of Soil Moisture in Agriculture. *International Journal of Combinatorial Optimization Problems and Informatics*, **15**, 61-71. https://doi.org/10.61467/2007.1558.2024.v15i4.502

[18] Taheri, M., Bigdeli, M., Imanian, H. and Mohammadian, A. (2025) An Overview of Machine-Learning Methods for Soil Moisture Estimation. *Water*, **17**, Article 1638. https://doi.org/10.3390/w17111638

[19] Bekele, D., Gela, A., Mengistu, D. and Derseh, A. (2023) Remote Sensing Based Soil Moisture Estimation for Agricultural Productivity: A Note from Lake Tana Sub Basin, NW Ethiopia. In: *New Insights in Soil-Water Relationship*, IntechOpen, 10. https://doi.org/10.5772/intechopen.109420

[20] Chen, L., Hu, B., Sun, J., Xu, Y.J., Zhang, G., Ma, H., *et al.* (2025) Using Remote Sensing and Machine Learning to Generate 100-Cm Soil Moisture at 30-M Resolution for the Black Soil Region of China: Implication for Agricultural Water Management. *Agricultural Water Management*, **309**, Article 109353. https://doi.org/10.1016/j.agwat.2025.109353

[21] Jet Propulsion Laboratory (n.d.) SMAP Observatory—Overview. NASA. https://smap.jpl.nasa.gov/observatory/overview/

[22] Suman, S., Srivastava, P.K., Petropoulos, G.P., Pandey, D.K. and O'Neill, P.E. (2020) Appraisal of SMAP Operational Soil Moisture Product from a Global Perspective. *Remote Sensing*, **12**, Article 1977. https://doi.org/10.3390/rs12121977

[23] Reichle, R.H., Liu, Q., Koster, R.D., Crow, W.T., De Lannoy, G.J.M., Kimball, J.S., *et al.* (2019) Version 4 of the SMAP Level-4 Soil Moisture Algorithm and Data Product. *Journal of Advances in Modeling Earth Systems*, **11**, 3106-3130. https://doi.org/10.1029/2019ms001729

[24] Mu, T., Liu, G., Yang, X. and Yu, Y. (2023) Soil-Moisture Estimation Based on Multiple-Source Remote-Sensing Images. *Remote Sensing*, **15**, Article 139. https://doi.org/10.3390/rs15010139

[25] Urban, M., Berger, C., Mudau, T.E., Heckel, K., Truckenbrodt, J., Onyango Odipo, V., *et al.* (2018) Surface Moisture and Vegetation Cover Analysis for Drought Monitoring in the Southern Kruger National Park Using Sentinel-1, Sentinel-2, and Landsat-8. *Remote Sensing*, **10**, Article 1482. https://doi.org/10.3390/rs10091482

[26] Wang, Q., Li, J., Jin, T., Chang, X., Zhu, Y., Li, Y., *et al.* (2020) Comparative Analysis of Landsat-8, Sentinel-2, and GF-1 Data for Retrieving Soil Moisture over Wheat Farmlands. *Remote Sensing*, **12**, Article 2708. https://doi.org/10.3390/rs12172708

[27] Entezari, M., Esmaeily, A. and Niazmardi, S. (2019) Estimation of Soil Moisture and Earth'S Surface Temperature Using Landsat-8 Satellite Data. *The International Archives of the Photogrammetry, Remote Sensing and Spatial Information Sciences*, **4**, 327-330. https://doi.org/10.5194/isprs-archives-xlii-4-w18-327-2019

[28] Tajudin, N., Ya'acob, N., Mohd Ali, D. and Adnan, N.A. (2021) Soil Moisture Index Estimation from Landsat 8 Images for Prediction and Monitoring Landslide Occurrences in Ulu Kelang, Selangor, Malaysia. *International Journal of Electrical and Computer Engineering*, **11**, Article 2101. https://doi.org/10.11591/ijece.v11i3.pp2101-2108

[29] Tao, L., Ryu, D., Western, A. and Boyd, D. (2021) A New Drought Index for Soil Moisture Monitoring Based on MPDI-NDVI Trapezoid Space Using MODIS Data. *Remote Sensing*, **13**, Article 122. https://doi.org/10.3390/rs13010122

[30] Tao, L., Di, Y., Wang, Y. and Ryu, D. (2023) Normalized Temperature Drought Index (NTDI) for Soil Moisture Monitoring Using MODIS and Landsat-8 Data. *Remote*

Sensing, **15**, Article 2830. https://doi.org/10.3390/rs15112830

[31] Tibkaew, A.P., Miyai, J., Buakhao, W. and Phonekeo, V. (2022) Soil Moisture Sensor Measurement and Vegetation-Soil-Water Related Indices—A Case Study in Mango Plantation, Nakhorn Ratchasima Province, Thailand. *International Journal of Geoinformatics*, **18**, 71-90.

[32] Lamichhane, M., Mehan, S. and Mankin, K.R. (2025) Soil Moisture Prediction Using Remote Sensing and Machine Learning Algorithms: A Review on Progress, Challenges, and Opportunities. *Remote Sensing*, **17**, Article 2397. https://doi.org/10.3390/rs17142397

[33] Malakhov, D. and Tsychuyeva, N. (2020) Calculation of the Biophysical Parameters of Vegetation in an Arid Area of South-Eastern Kazakhstan Using the Normalized Difference Moisture Index (NDMI). *Central Asian Journal of Environmental Science and Technology Innovation*, **4**, 189-198.

[34] Welikhe, P., Quansah, J.E., Fall, S. and McElhenney, W. (2017) Estimation of Soil Moisture Percentage Using Landsat-Based Moisture Stress Index. *Journal of Remote Sensing & GIS*, **6**, Article 1000200.

[35] Li, M., Sun, H. and Zhao, R. (2023) A Review of Root Zone Soil Moisture Estimation Methods Based on Remote Sensing. *Remote Sensing*, **15**, Article 5361. https://doi.org/10.3390/rs15225361

[36] Peng, J. and Loew, A. (2017) Recent Advances in Soil Moisture Estimation from Remote Sensing. *Water*, **9**, Article 530. https://doi.org/10.3390/w9070530

[37] Babaeian, E. and Tuller, M. (2023) The Feasibility of Remotely Sensed Near-Infrared Reflectance for Soil Moisture Estimation for Agricultural Water Management. *Remote Sensing*, **15**, Article 2736. https://doi.org/10.3390/rs15112736

[38] Celik, M.F., Isik, M.S., Yuzugullu, O., Fajraoui, N. and Erten, E. (2022) Soil Moisture Prediction from Remote Sensing Images Coupled with Climate, Soil Texture and Topography via Deep Learning. *Remote Sensing*, **14**, Article 5584. https://doi.org/10.3390/rs14215584

[39] Mohanty, B.P., Cosh, M.H., Lakshmi, V. and Montzka, C. (2017) Soil Moisture Remote Sensing: State-of-the-Science. *Vadose Zone Journal*, **16**, 1-9. https://doi.org/10.2136/vzj2016.10.0105

[40] Chen, Y., Palta, J.A., Wu, P. and Siddique, K.H.M. (2019) Crop Root Systems and Rhizosphere Interactions. *Plant and Soil*, **439**, 1-5. https://doi.org/10.1007/s11104-019-04154-2

[41] S.1643-117th Congress (2021–2022): Alabama Black Belt National Heritage Area Act (2021-05-13). https://www.congress.gov/bill/117th-congress/senate-bill/1643

[42] Quansah, J., Doria, R. and Fall, S. (2025) Evaluating the Performance of the National Water Model: A Spatiotemporal Analysis of Streamflow Forecasting. *Water*, **17**, Article 2950. https://doi.org/10.3390/w17202950

[43] Winemiller, T. (2009) Black Belt Region in Alabama. https://encyclopediaofalabama.org/article/black-belt-region-in-alabama/

[44] Smith, E.A., Johnson, L.C., Langdon Jr, D.W., Aldrich, T.H. and Cunningham, K.M. (1894) Report on the Geology of the Coastal Plain of Alabama. https://books.google.com/books?id=BzsxAQAA-MAAJ&printsec=frontcover&source=gbs_ge_summary_r&cad=0#v=onepage&q&f=false

[45] Stephenson, L.W. and Monroe, W.H. (1938) Stratigraphy of Upper Cretaceous Series in Mississippi and Alabama. *AAPG Bulletin*, **22**, 1639-1657.

https://doi.org/10.1306/3d933022-16b1-11d7-8645000102c1865d

[46] Soil Survey Staff, Natural Resources Conservation Service, United States Department of Agriculture (2025) Web Soil Survey. http://websoilsurvey.sc.egov.usda.gov/

[47] USDA NASS (2010) Field Crops Usual Planting and Harvesting Dates (Agricultural Handbook 628). United States Department of Agriculture. https://esmis.nal.usda.gov/sites/default/release-files/vm40xr56k/dv13zw65p/w9505297d/planting-10-29-2010.pdf

[48] Alabama Cooperative Extension System (2018) Planting Guide for Home Gardening in Alabama (ANR-0063). https://www.aces.edu/blog/topics/lawn-garden/planting-guide-for-home-gardening-in-alabama/

[49] NASA (2023) Harmonized Landsat and Sentinel-2 (HLS). https://hls.gsfc.nasa.gov/

[50] Ju, J., Zhou, Q., Freitag, B., Roy, D.P., Zhang, H.K., Sridhar, M., *et al.* (2025) The Harmonized Landsat and Sentinel-2 Version 2.0 Surface Reflectance Dataset. *Remote Sensing of Environment*, **324**, Article 114723. https://doi.org/10.1016/j.rse.2025.114723

[51] Gorelick, N., Hancher, M., Dixon, M., Ilyushchenko, S., Thau, D. and Moore, R. (2017) Google Earth Engine: Planetary-Scale Geospatial Analysis for Everyone. *Remote Sensing of Environment*, **202**, 18-27. https://doi.org/10.1016/j.rse.2017.06.031

[52] Google Earth Engine (n.d.) Earth Engine Data Catalog. https://developers.google.com/earth-engine/datasets

[53] Earth Resources Observation and Science (EROS) Center (2020) Landsat 8-9 Operational Land Imager/Thermal Infrared Sensor Level-2, Collection 2 [Dataset]. U.S. Geological Survey. https://doi.org/10.5066/P9OGBGM6

[54] European Space Agency (n.d.) Sentinel-2. https://www.esa.int/Applications/Observing_the_Earth/Copernicus/Sentinel-2

[55] European Space Agency (2026) Sentinel-2 Level 2A Surface Reflectance. Copernicus Data Space Ecosystem Documentation. https://documentation.dataspace.copernicus.eu/Data/SentinelMissions/Sentinel2.html#sentinel-2-level-2a-surface-reflectance

[56] U.S. Geological Survey (n.d.) Normalized Difference Moisture Index (NDMI). https://www.usgs.gov/landsat-missions/normalized-difference-moisture-index

[57] SciPy Developers (2026) Statistical Functions (Scipy.Stats). SciPy. https://docs.scipy.org/doc/scipy-1.17.0/reference/stats.html

[58] Shaqiri, M., Iljazi, T., Kamberi, L. and Ramani-Halili, R. (2023) Differences between the Correlation Coefficients Pearson, Kendall and Spearman. *Journal of Natural Sciences and Mathematics of UT*, **8**, 392-397

[59] El-Hashash, E.F. and Shiekh, R.H.A. (2022) A Comparison of the Pearson, Spearman Rank and Kendall Tau Correlation Coefficients Using Quantitative Variables. *Asian Journal of Probability and Statistics*, **20**, 36-48. https://doi.org/10.9734/ajpas/2022/v20i3425

[60] Wang, H., Muller, J.D., Tatarinov, F., Yakir, D. and Rotenberg, E. (2022) Disentangling Soil, Shade, and Tree Canopy Contributions to Mixed Satellite Vegetation Indices in a Sparse Dry Forest. *Remote Sensing*, **14**, 3681. https://doi.org/10.3390/rs14153681

[61] METER Group (n.d.) TEROS 12—Advanced Soil Moisture Sensor+Temperature and EC. https://metergroup.com/products/teros-12/

[62] Markham, B., Barsi, J., Kvaran, G., Ong, L., Kaita, E., Biggar, S., *et al.* (2014) Landsat-8 Operational Land Imager Radiometric Calibration and Stability. *Remote Sensing*, **6**, 12275-12308. https://doi.org/10.3390/rs61212275

[63] Optical Mission Performance Cluster Service (2025) Data Quality Report—Sentinel-2 MSI L2A (Issue 87.0, OMPC.CS.DQR.002.06-2025). Copernicus Space Component. https://sentiwiki.copernicus.eu/__attachments/1673423/OMPC.CS.DQR.002.06-2025-Sentinel-2-MSI-L2A-DQR-July-2025-87.pdf?inst-v=d0190039-b174-4e67-b630-27bc085e66cf